Bioelectrochemistry 131 (2020) 107395

Contents lists available at ScienceDirect

Bioelectrochemistry

journal homepage: www.elsevier.com/locate/bioelechem

Effect of electrode spacing on electron transfer and conductivity of *Geobacter sulfurreducens* biofilms

Panpan Liu [a,b], Abdelrhman Mohamed [b], Peng Liang [a], Haluk Beyenal [b,*]

[a] State Key Joint Laboratory of Environment Simulation and Pollution Control School of Environment, Tsinghua University, Beijing 100084, PR China
[b] The Gene and Voiland School of Chemical Engineering and Bioengineering, Washington State University, Pullman, WA 99163, USA

ARTICLE INFO

Article history:
Received 15 April 2019
Received in revised form 12 September 2019
Accepted 13 September 2019
Available online 4 October 2019

Keywords:
Electrochemically active biofilm
Exoelectrogens
Biofilm conductivity
Extracellular electron transfer
Microbial electrochemistry and spatial heterogeneity

ABSTRACT

To understand electron transport in electrochemically active biofilms, it is necessary to elucidate the heterogeneous electron transport across the biofilm/electrode interface and in the interior of *G. sulfurreducens* biofilms bridging gaps of varying widths. The conductivity of *Geobacter sulfurreducens* biofilm bridging nonconductive gaps with widths of 5 μm, 10 μm, 20 μm and 50 μm is investigated. Results of electrochemical gating measurement show that biofilm conductivity peaks at the potential of −0.35 V vs. Ag/AgCl. The biofilm conductivity increases with gap width (10.4 ± 0.2 μS cm^{-1} in 5 μm gap, 13.3 ± 0.2 μS cm^{-1} in 10 μm gap, 16.7 ± 1.4 μS cm^{-1} in 20 μm gap and 41.8 ± 2.02 μS cm^{-1} in 50 μm gap). These results revealed that electron transfer in *G. sulfurreducens* biofilm is a redox-driven. In addition, higher biofilm conductivities and lower charge transfer resistances are observed in all gaps under a turnover condition than in those under a non-turnover condition. Our results offer insights into the spatial heterogeneity of biofilm structure and extracellular electron transfer in electrochemically active biofilms.

1. Introduction

Exoelectrogens are microorganisms that can oxidize organic matter and use an inert electrode as an electron acceptor [1]. This trait allows their use as live catalysts in bioelectrochemical systems, such as microbial fuel cells, microbial desalination cells, microbial biosensors and microbial electrolysis cells [2–5]. In general, exoelectrogens in a bioelectrochemical system colonize the electrode surface and form an electrochemically active biofilm (EAB) which catalyzes the substrate consumption reaction and delivers the metabolic electrons to the electrode. The efficiency of electron transfer in an EAB determines the performance of the bioelectrochemical system [6]. Determining the electron transport rates in biofilms can advance the application of bioelectrochemical systems. It is well established that extracellular electron transfer (EET) performed by model exoelectrogen *Geobacter sulfurreducens* is mediated by three different electrochemically active cellular components: outer membrane cytochromes, conductive pili and electron shuttles [7,8]. However, as a multicell EAB forms on an electrode, electrons produced by exoelectrogens far from the electrode surface must span the multicell, layered biofilm. The diverse electrochemically active constituents in an EAB make the EET in biofilm challenging to measure directly and analyze over long distances.

Long-distance electron transport in biofilms was previously proposed to be mediated by electrochemically active constituents including outer membrane cytochrome, pili, and extracellular polymeric substances [8–11]. As the adaptation to the local microenvironment and the production of electrochemically active constituents by exoelectrogens vary with the distance from the electrode surface, their abundance is nonuniform throughout the biofilm [12]. As a result, EABs develop a heterogeneous spatial structure and the characteristics of electron transport in biofilm are dependent on the distance from the electrode surface [13,14].

Biofilm conductivity was previously measured to indicate long-range electron transfer in biofilm [15,16]. Previous studies measured the biofilm conductance of mixed-culture and *G. sulfurreducens* biofilms using split electrodes with 50–μm to 1–mm nonconductive gaps in various microbial fuel cells [17,18]. While these results emphasized that biofilms can conduct electrons spanning these nonconductive distances, they did not reveal whether the biofilm conductivity depended on the nonconductive gap width [8,17,19,20]. Moreover, there was a lack of

* Corresponding author.
E-mail address: beyenal@wsu.edu (H. Beyenal).

https://doi.org/10.1016/j.bioelechem.2019.107395
1567-5394/

comprehensive comparison of electron transport over different distances. Recent research found heterogeneous electron transport across the biofilm is highly correlated with structure in *G. sulfurreducens* biofilm using the interdigitated array electrode [21]. The gap width of 5 μm was too short to reveal the effect of distance on the electron transport in biofilm which had a thickness more than 50 μm.

To understand electron transport in EAB, it is necessary to elucidate the heterogeneous electron transport across the biofilm/electrode interface and in the interior of *G. sulfurreducens* biofilm by bridging gaps of varying widths. We expect that this information will explain the dependence of electron transfer processes in biofilms on a variety of nonconductive gap widths.

The goal of this research was to investigate the conductivity and electron transport of *G. sulfurreducens* biofilm by varying electrode spacing. A split gold electrode with nonconductive gaps with widths of 5 μm, 10 μm, 20 μm and 50 μm was fabricated, and model exoelectrogen *G. sulfurreducens* biofilm was grown on it until the turnover current reached a steady state and the biofilm bridged the nonconductive gaps. Biofilm conductivities were measured across these gaps and related to the gap widths. Bipotentiostat electrochemical gating measurements were performed to examine the change of biofilm conductivity with the electrode potential.

2. Methods and materials

2.1. Fabrication of the split gold electrode

A split gold electrode with nonconductive gaps of 5 μm, 10 μm, 20 μm and 50 μm was designed to perform *in situ* measurement of biofilm conductivity. The electrode fabrication was adapted from a previous study [8]. Briefly, electrodes with different nonconductive gaps were prepatterned on a Si/SiO_2 wafer and then defined using electron-beam lithography (EBL). A layer of 20 nm of Ti and 200–nm Au was spurted onto the electrodes by evaporation. The whole electrode was 2 cm long and about 5 cm wide (Fig. S1). Electrodes were wired with copper conductor by soldering them together with 60:40 tin/lead solder. The connecting joints were covered with silicone to prevent corrosion due to exposure of solder to growth medium. Before being placed into a reactor, the split electrode was soaked in 3% acetone for 30 min, followed by rinsing with ethanol for 1 h to clean the surface, then rinsed with deionized water.

2.2. G. sulfurreducens enrichment and biofilm growing

G. sulfurreducens strain PCA (ATCC 51573) was first grown in a serum vial with an anaerobic medium: KCl, 0.38 g L^{-1}; NH_4Cl, 0.2 g L^{-1}; Na_2HPO_4, 0.069 g L^{-1}; $CaCl_2$, 0.04 g L^{-1}; $ZnSO_4 \cdot 7H_2O$, 0.2 g L^{-1}; $NaHCO_3$, 2 g L^{-1}; Wolfe's vitamin solution, 10 mL L^{-1}; modified Wolfe's mineral solution, 10 mL L^{-1}. The electron donor was 20 mM sodium acetate, and the electron acceptor was 40 mM fumarate [22]. The starting cultures were ready for inoculation when there was a visible pink layer of cells at the bottom of the vial. Prior to inoculation, the reactor and growth medium were autoclaved for 20 min at 121 °C. After cooling to room temperature, the reactor was placed in an incubator set to 30 ± 1 °C. The reactor was sparged with mixed gas (80%/20% N_2/CO_2) for 24 h to remove oxygen from the system. The working electrode was polarized at +0.2 V vs. Ag/AgCl using a custom-made potentiostat [23]. Then 10 mL of cell suspension was injected into each reactor.

Two reactors were built to grow the biofilm, and each was assembled with a split gold electrode as the working electrode. The reactors were made of glass and had a working volume of 250 mL. Tygon tubing (Cole-Parmer, Vernon Hills, IL, catalog EW-06475-14, EW-06475-16) with a 0.2-μm filter was used at the gas inlet to sparge N_2/CO_2 (80%/20%) mixed gas (Fig. S1). Reactor pressure was built up by using another 0.2-μm filter gas outlet. The reactor was operated in batch mode. The split gold electrode, an Ag/AgCl electrode and a graphite rod were used as the working electrode, reference electrode and counter electrode, respectively. We used one split electrode which included all the gaps as a single working electrode (Fig. S1). However, during the measurements, we only used the given gap distance. The growth medium did not contain any electron acceptor, and only 20 mM sodium acetate was used as the electron donor. The conductivity of the fresh growth medium was 5.11 mS cm^{-1}.

2.3. Biofilm conductance measurement

In the process of biofilm formation on the electrode, electrochemical measurements to characterize the biofilms were performed using a potentiostat (Gamry Instruments Inc. G300™). Before each measurement, the working electrode was disconnected for 60 min to allow it to reach a steady state. Cyclic voltammetry (CV) was conducted on the working electrode. The scan window ranged from −0.7 V vs. Ag/AgCl to +0.4 V vs. Ag/AgCl at a rate of 10 mV s^{-1}. The first derivative of CV was obtained by plotting the slope of each CV point against the scan potential. To measure the conductance of the biofilm, a voltage difference (V_{SD}, 0 mV, 25 mV, or 50 mV) was applied to the gaps. For each voltage, a long period of 5 min was applied to allow the transient current to decay. Current (I_{SD}) was recorded every second over the 5–min period, and the conductance of the biofilm was calculated using the values I_{SD} with V_{SD}. For Electrochemical Impedance Spectroscopy (EIS) measurement of the biofilm at the various gaps, one side of the gap (source electrode) was used as the working electrode, and the other side (drain electrode) was used as the reference and counter electrode. The open circuit potential was used as the DC potential, and the AC potential was 10 mV rms. The frequency range was from 100 mHz to 100,000 Hz with 10 points of data acquisition. Zview software (Scribner Associates Inc., Southern Pines, NC, USA) was used to analyze biofilm impedance obtained from EIS results. For the measurement of each gap, a period of 30 min was used to recover the current production of the biofilm.

2.4. Electrochemical gating measurements to estimate biofilm conductivity at various applied gating potentials

Electrochemical gating measurements were performed using Gamry's bipotentiostat setup containing two Interface 1000E potentiostats (Gamry Instruments, Warminster, PA). These are two fully functional potentiostats whose timing has been synchronized; they share reference and counter electrodes. For the bipotentiostat electrochemical gating measurements, the source and drain electrodes at each end of the nonconductive gap in the split gold electrode were used as the working electrodes of the two fully functional potentiostats simultaneously. The Ag/AgCl reference electrode and the graphite rod were used as the reference electrode and the counter electrode, respectively. The average potential between the source and drain working electrodes is termed the gate potential. The gate potential was linearly swept between −0.7 V vs. Ag/AgCl and +0.4 V vs. Ag/AgCl at a rate of 10 mV/s. Simultaneously, a source-drain potential (V_{SD}) of 0 mV or 50 mV was maintained between the source and drain electrodes. Repeated scans were recorded to minimize the effect of transient current. The currents of source (I_{source}) and drain (I_{drain}) electrodes were recorded for 2 CV cycles. Biofilm conductance was calculated by fitting ΔI and V_{SD}. The measurements were performed with and without substrate oxidation (turnover condition/non-turnover condition). To obtain the non-turnover condition, first the medium in the bioreactor was replaced with growth medium without sodium acetate and then the working electrode was polarized at +0.2 V vs. Ag/AgCl until the current decreased to below 5 μA.

2.5. Confocal laser scanning microscopy of the G. sulfurreducens biofilm

At the end of the experiment, the electrode covered with *G. sulfurreducens* biofilm was carefully taken out. The whole electrode was then stained with a live/dead BacLight Bacterial Viability Kit (Molecular Probes, Eugene, OR, USA) following the instructions of the manufacturer. Stained specimens were then imaged using a Nikon C1 confocal microscope (Eclipse TE200, Nikon, Tokyo, Japan) with a 10× objective lens. The biofilm images were taken using the NIS-element software (Nikon, Tokyo, Japan), and the average biofilm thickness was estimated using the software.

2.6. Biofilm conductivity calculation

Biofilm conductivity was calculated according to the method used in a previous study [18]. The following equation was used:

$$\sigma = G\frac{\pi}{L}/ln\left(\frac{8g}{\pi a}\right), \quad (1)$$

where σ is the biofilm conductivity, g is the biofilm thickness, a is the half width of nonconductive gaps, G is the experimentally measured biofilm conductance and L is the length of the electrode.

3. Results and discussion

3.1. Electrochemical activity changes with the growth of G. Sulfurreducens biofilm

Current production started to increase ~1.5 days after *G. sulfurreducens* inoculation. This was followed by an exponential phase and a plateau which was observed after ~5 days (Fig. 1A). A second plateau of current production was observed at ~25 days, indicating the further growth of biofilm on the electrode. During the biofilm formation on the electrode, CVs and biofilm conductance were measured on different days (Fig. 1B, C and D). A typical sigmoid-type CV was observed for biofilm at each selected monitoring point (Fig. 1B). Under these conditions, the potential at which current began to increase ranged from −0.37 V vs. Ag/AgCl at 5 d to −0.48 V vs. Ag/AgCl at 20 d, and the rate of electron transport in the biofilm rose rapidly after this potential. Limiting currents were obtained above −0.29 V vs. Ag/AgCl at 5 d and above −0.19 V vs. Ag/AgCl at 20 d as the biofilm grew. Similar CVs were observed after 20 days of electrode-attached culture growth, which indicated stable electrochemical activity of the biofilm after 20 d. The first-order derivative analysis of CVs indicated the inflection point of biofilm catalytic behavior, and curves for various days are shown in Fig. S2. Two dominant peaks were imaged by the analysis, and these increased in height with biofilm growth (Fig. 1C). The midpoint potential of −0.35 V vs. Ag/AgCl of the two symmetrical peaks indicated that there was one oxidation/reduction event in electron transport [24]. One smaller intensity peak, centered at −0.38 V vs. Ag/AgCl, was detected. This peak was also found for the *G. sulfurreducens* biofilm growing on glassy carbon electrodes [24]. The potential of the smaller peak can be compared to the midpoint potential of multiheme cytochromes involved in *G. sulfurreducens* electron transport, such as periplasmic cytochrome *c* purified from *G. sulfurreducens* (−0.37 V vs. Ag/AgCl) [25]. Initial increases in biofilm conductance at all distances were correlated to increases of current production (Fig. 1D). After 25 days of attachment, the obtained stable conductance of the biofilm was 0.078 ± 0.007 mS in the 5-μm gap, 0.085 ± 0.011 mS in the 10–μm gap, 0.088 ± 0.006 mS in the 20–μm gap and 0.090 ± 0.008 mS in the 50–μm gap, suggesting that mature biofilm bridged all nonconductive gaps. A smaller biofilm conductance was obtained in the 5-μm gap (0.078 ± 0.007 mS) than in the other three gaps (Fig. 1D). The highest biofilm conductance obtained was 0.090 ± 0.008 mS in the

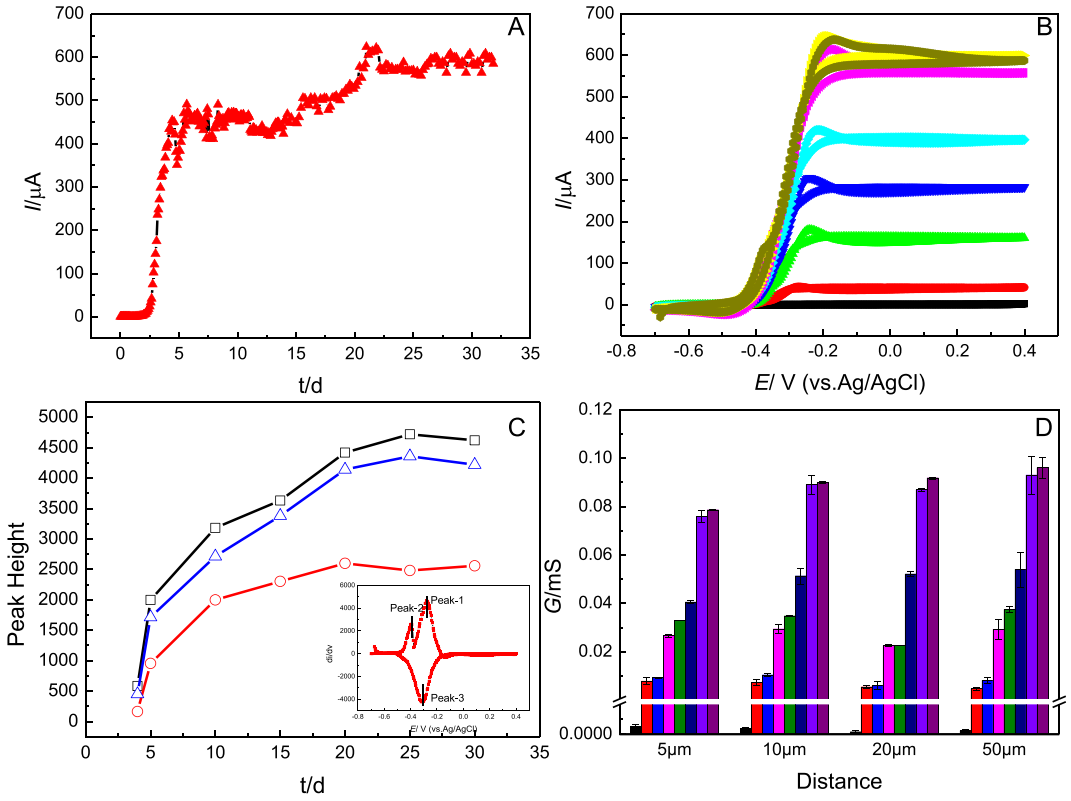

Fig. 1. (A) Current production of *G. sulfurreducens* biofilm over the whole split electrode including all gaps, (B) CVs of biofilm on various days (in A), (C) heights of first-derivatives peaks of CVs of biofilms (black square, peak-1, red circle, peak-2, blue triangle, peak-3), and (D) biofilm conductance measured on various days for the data given in Figure A.

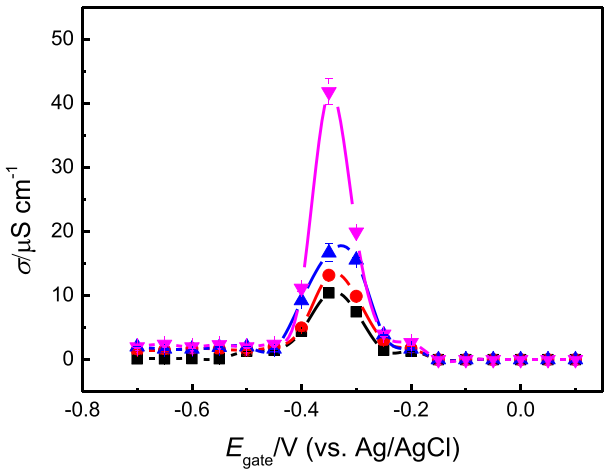

Fig. 2. Biofilm conductivity varying with gate potential in four nonconductive gaps (black square, 5 μm, red circle, 10 μm, blue up triangle, 20 μm, magenta down triangle, 50 μm).

50–μm gap, which is comparable to the result obtained in a previous study [18].

3.2. Electrochemical gating measurements revealed redox-driven electron transfer in biofilm bridging gaps with different widths

Biofilm images were acquired using a confocal microscope, and the results are shown in Fig. S3. There was no gap observed at the top of the biofilm images, which indicates that biofilm bridged all four nonconductive gaps. Moreover, *G. sulfurreducens* biofilm attached to the electrode had a relatively uniform thickness, with an average biofilm thickness of approximately 113 μm. The variation of calculated biofilm conductivity with gate potential is shown in Fig. 2. Similar trends of biofilm conductivity varying with gate potential were observed for all four gaps. The highest conductivities at the gate potential of −0.35 V vs. Ag/AgCl were 10.4 ± 0.2 μS cm^{-1} in the 5–μm gap, 13.3 ± 0.2 μS cm^{-1} in the 10–μm gap, 16.7 ± 1.4 μS cm^{-1} in the 20–μm gap and 41.8 ± 2.0 μS cm^{-1} in the 50-μm gap, which suggests redox-driven electron transfer in biofilm in these gaps [26]. Redox-driven electron transfer in *G. sulfurreducens* biofilm was previously observed in a 5-μm gap using an interdigitated microelectrode array [27]. In another study, a different trend, in which biofilm conductivity increased with electrode potential, was observed using a 50-μm split electrode, supporting metallic-like mechanism in *Geobacter* biofilms and in extracted pili without involvement of cytochromes in biofilm conductivity [18,28]. The reason behind the disagreement in the results might be that the electrochemical gating measurements were conducted with different measurement methods [16]. In our experiments, the gating measurement was conducted by using two fully functional potentiostats whose timing has been synchronized. The potential of source and drain electrodes could be controlled accurately and the large background current from spilt electrode could be subtracted. Mechanistic studies to distinguish the contribution of pili and c-type cytochromes to long-range biofilm conductivity have been conducted. For example, β-mercaptoethanol was used as a cytochrome denaturing reagent to limit the contribution of cytochromes to biofilm-conductivity [18]. However, these results were contested as β-mercaptoethanol may not completely denature cytochromes which is required to stop their contribution to conductivity measurements [29].

The highest biofilm conductivity was obtained at the potential of −0.35 V vs. Ag/AgCl. This is comparable to the half-wave potential of CV curves, which represents the inflection point resulting from the possible contribution of multiple redox active couples [24]. In addition, biofilm conductivity increased with gap width, indicating a faster rate of electron transport in biofilm bridging larger gaps. There are several possible reasons for this result and they will be discussed in the following section.

Electrochemical gating measurement was also performed by sweeping the source and drain electrode potentials with a larger potential window (from −0.7 V vs. Ag/AgCl to +0.4 V vs. Ag/AgCl). The results are shown in Fig. S4. The difference in current production between source and drain electrodes at the gating voltage of 50 mV indicates electron transport in the biofilm between the source and drain electrodes (Fig. S4B, D, F and H). Using this method, accurate biofilm conductivity could not be obtained because of the high background capacitive currents [16]. Thus, in this study, a long period of electrode polarizing was used to allow the decay of the background current and was more suitable for obtaining the accurate biofilm conductivity.

3.3. Biofilm conductivity increases with the gap width

The varying of biofilm conductivity with the gap width is shown in Fig. 3A. Biofilm conductivity increased with gap width under the nonturnover condition (10.4 ± 0.2 μS cm^{-1} in the 5-μm gap, 13.3 ± 0.2 μS cm^{-1} in the 10-μm gap, 16.7 ± 1.4 μS cm^{-1} in the 20-μm gap and 41.8 ± 2.0 μS cm^{-1} in the 50-μm gap), indicating heterogeneous electron transport in *G. sulfurreducens* biofilm bridging gaps of various widths (Fig. 3A). Previous work by Malvankar et al. reported similar

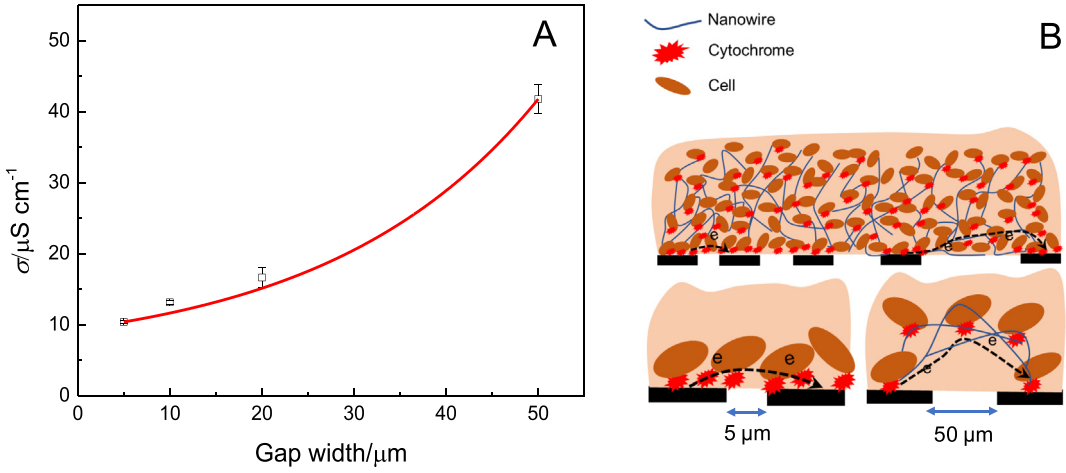

Fig. 3. (A) Biofilm conductance varying with gap width and (B) the proposed schematic of electron transport in biofilm in gaps with different widths.

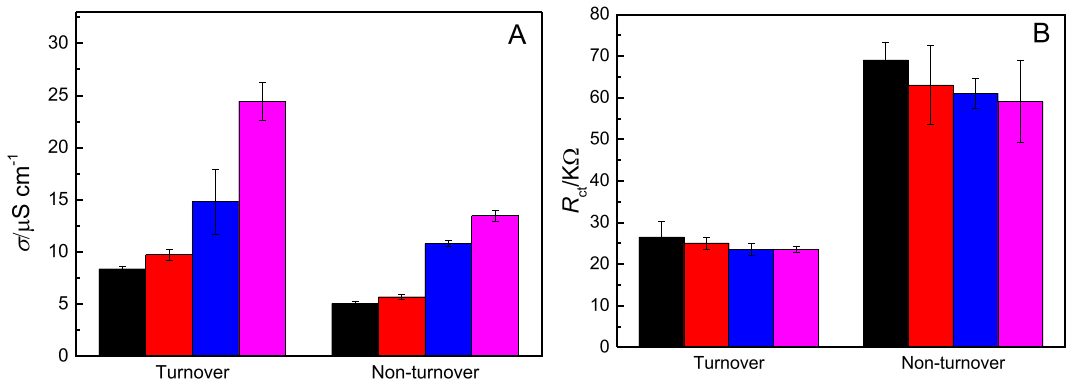

Fig. 4. (A) Conductivity and (B) charge transfer resistances of biofilm bridging the four gaps under a turnover and under a non-turnover condition (black, 5 μm, red, 10 μm, blue, 20 μm, magenta, 50 μm).

conductance values for *G. sulfurreducens* DL-1 biofilms bridging gaps of 50 μm and 100 μm (exact values not reported) [6]. A mechanistic explanation for the observed increase in wider gaps is not determined. The observed increase in biofilm conductivity may indicate an adaptation mechanism of *G. sulfurreducens* biofilm, in which the larger width gap is a challenge for biofilm bridging. It is possible that *G. sulfurreducens* overexpresses conductive pili or c-type cytochromes to cover the larger gaps. This could increase the conductivity of biofilms with a large gap (41.8 ± 2.0 μS cm^{-1} in the 50-μm gap) (Fig. 3B). This speculation coincides with the previous finding that expression of the pili is required to maintain electrical connectivity as cell grows far from the electrode surface, especially for biofilm thicknesses beyond ~10 μm [30]. In addition, the electrochemical activity of biofilm with pili was much higher (~2-fold) than that without pili even when the biofilm thickness, number of viable cells and outer membrane cytochrome were similar [30]. Thus, we speculate that the higher biofilm conductivity in larger gaps is attributable to the overexpression of pili or c-type cytochromes. Another possibility is the existence of a proton gradient among gaps with different widths. In a large gap (i.e. 50 μm), biofilm has a lower overall metabolic activity, which would lead to a more neutral local pH in the gap. Redox protein in this gap would be more active, explaining the higher biofilm conductivity (41.8 ± 2.0 μS cm^{-1}) obtained in the 50-μm gap in comparison to the smaller gaps (10.4 ± 0.2 μS cm^{-1} in the 5-μm gap). It has been reported that for the gaps width bigger than 50 μm, electron transport in biofilm mediated by c-type cytochromes or pili and similar conductance was observed [6,17].

Nevertheless, the electrochemical gating results suggest redox-driven electron transport in biofilm in all gap widths (Fig. 2). There are two reasons for this result. One is that multiheme c-type cytochrome preferentially localizes closer to the electrode and on its surface [31], which functions as an electrochemical gate between the *G. sulfurreducens* biofilm and the electrode. In addition, the conductive pili and the cytochromes work coordinately as electron carriers to maintain optimal rates of electron transfer in *G. sulfurreducens* biofilm [30]. Thus, the same trend of biofilm conductivity varying with electrode potential was found for biofilm in all these gaps. The other reason might be that some conductive *G. sulfurreducens* pili are composed solely of c-type cytochrome, which would also lead redox-driven electron transport over a long distance in *G. sulfurreducens* biofilm [32,33]. Such as the use of mutants (e.g., OmcZ and OmcS) can be used to understand contributions of key cytochromes to biofilm conductivity when the gap distance increase.

3.4. Conductivity and charge transport resistance of biofilm under turnover and non-turnover conditions

A comparison of conductivity and charge transfer resistance in biofilm under a turnover condition (with substrate) and a non-turnover condition (without substrate) was shown in Fig. 4. Higher biofilm conductivity (8.4 ± 0.2 μS cm^{-1} in a 5-μm gap, 9.7 ± 0.6 μS cm^{-1} in a 10-μm gap, 14.8 ± 3.1 μS cm^{-1} in a 20-μm gap and 24.4 ± 1.7 μS cm^{-1} in a 50-μm gap) was obtained under turnover conditions than under non-turnover conditions (5.0 ± 0.3 μS cm^{-1} in a 5-μm gap, 5.6 ± 0.2 μS cm^{-1} in a 10-μm gap, 10.7 ± 0.3 μS cm^{-1} in a 20-μm gap and 13.4 ± 0.5 μS cm^{-1} on 50 μm gap) (Fig. 4A). With substrate oxidation, the metabolic electrons could result in a larger measured source-drain current and lead to a higher biofilm conductivity [33]. In addition, biofilm structure changed during the long starve period for obtaining the non-turnover condition, and then decreased biofilm conductivities were obtained [8]. The decrease of biofilm conductance under the non-turnover condition was also observed for mixed-culture EAB [34,35]. These results could provide insight into how microbial activity and electron production influence biofilm conductivity [26]. EIS measurement was further used to determine the total charge transfer resistance of biofilm in the four gaps. Coincidentally, the charge transfer resistances of biofilm under the turnover condition (26.4 ± 3.8 KΩ in a 5-μm gap, 25.0 ± 1.5 KΩ in a 10-μm gap, 23.5 ± 1.5 KΩ in a 20-μm gap and 23.6 ± 0.7 KΩ in a 50-μm gap) were lower than those without substrate oxidation (69.0 ± 8.2 KΩ in a 5-μm gap, 63.4 ± 9.6 KΩ in a 10-μm gap, 61.3 ± 2.6 KΩ in a 20-μm gap and 59.1 ± 7.8 KΩ in a 50-μm gap) (Fig. 4B), which indicates faster electron transport in biofilm with substrate oxidation. Furthermore, larger charge transfer resistances were observed for the biofilm bridging the gaps with smaller widths under either a turnover or a non-turnover condition, indicating that electron transport efficiency increases with electrode spacing.

4. Conclusions

In this study, the conductivities of *G. sulfurreducens* biofilm bridging nonconductive gaps with widths of 5 μm, 10 μm, 20 μm and 50 μm were determined. Bipotentiostat electrochemical gating measurement showed the highest biofilm conductivities (10.4 ± 0.2 μS cm^{-1} in a 5-μm gap, 13.3 ± 0.2 μS cm^{-1} in a 10-μm gap, 16.7 ± 1.4 μS cm^{-1} in a 20-μm gap and 41.8 ± 2.0 μS cm^{-1} in a 50-μm gap) at the potential of −0.35 V vs. Ag/AgCl and revealed that electron transfer in biofilm is a redox-driven adaptation mechanism of *G. sulfurreducens* biofilm, in which the expression of cytochrome and pili depends on the electrode spacing. Biofilm conductivity increased with gap width. Moreover, in all gaps higher biofilm conductivity and lower charge transfer resistance were obtained under the turnover condition than under the non-turnover condition, revealing that electron transport in biofilm may be influenced by microbial activity.

Declaration of Competing Interest

The authors have no competing interests to declare.

Acknowledgements

This work was supported by the National Science Foundation of United States, award #1706889 and National Science Foundation of China (NSFC No. 51778324, 51422810). The authors gratefully acknowledge financial support from the China Scholarship Council.

Appendix A. Supplementary material

Supplementary data to this article can be found online at https://doi.org/10.1016/j.bioelechem.2019.107395.

References

[1] R. Kumar, L. Singh, A.W. Zularisam, Exoelectrogens: Recent advances in molecular drivers involved in extracellular electron transfer and strategies used to improve it for microbial fuel cell applications, Renew. Sust. Energ. Rev. 56 (2016) 1322–1336.
[2] P. Liu, P. Liang, Y. Jiang, W. Hao, B. Miao, D. Wang, X. Huang, Stimulated electron transfer inside electroactive biofilm by magnetite for increased performance microbial fuel cell, Appl. Energy 216 (2018) 382–388.
[3] Y. Jiang, X. Yang, P. Liang, P. Liu, X. Huang, Microbial fuel cell sensors for water quality early warning systems: Fundamentals, signal resolution, optimization and future challenges, Renew. Sust. Energ. Rev. 81 (2018) 292–305.
[4] X.X. Cao, X. Huang, P. Liang, K. Xiao, Y.J. Zhou, X.Y. Zhang, B.E. Logan, A new method for water desalination using microbial desalination cells, Environ. Sci. Technol. 43 (2009) 7148–7152.
[5] P. Liu, C. Zhang, P. Liang, Y. Jiang, X. Zhang, X. Huang, Enhancing extracellular electron transfer efficiency and bioelectricity production by vapor polymerization Poly (3,4-ethylenedioxythiophene)/MnO2 hybrid anode, Bioelectrochemistry 126 (2018) 72–78.
[6] N.S. Malvankar, M.T. Tuominen, D.R. Lovley, Biofilm conductivity is a decisive variable for high-current-density Geobacter sulfurreducens microbial fuel cells, Energy Environ. Sci. 5 (2012) 5790.
[7] A. Kumar, L.H.-H. Hsu, P. Kavanagh, F. Barrière, P.N.L. Lens, L. Lapinsonnière, J.H. Lienhard, V.U. Schröder, X. Jiang, D. Leech, The ins and outs of microorganism–electrode electron transfer reactions, Nat. Rev. Chem. 1 (2017) 0024.
[8] M. Ding, H.Y. Shiu, S.L. Li, C.K. Lee, G. Wang, H. Wu, N.O. Weiss, T.D. Young, P.S. Weiss, G.C. Wong, K.H. Nealson, Y. Huang, X. Duan, Nanoelectronic investigation reveals the electrochemical basis of electrical conductivity in shewanella and geobacter, ACS Nano (2016).
[9] E. Marsili, D.B. Baron, I.D. Shikhare, D. Coursolle, J.A. Gralnick, D.R. Bond, Shewanella secretes flavins that mediate extracellular electron transfer, Proc. Natl. Acad. Sci. U. S. A. 105 (2008) 3968–3973.
[10] Y. Xiao, E. Zhang, J. Zhang, Y. Dai, Z. Yang, H.E.M. Christensen, J. Ulstrup, F. Zhao, Extracellular polymeric substances are transient media for microbial extracellular electron transfer, Sci. Adv. 3 (2017)e1700623.
[11] S.K. Sure, L.M. Ackland, A.A. Torriero, A. Adholeya, M. Kochar, Microbial nanowires: an electrifying tale, Microbiology (2016).
[12] D.R. Lovley, Electrically conductive pili: Biological function and potential applications in electronics, Curr. Opin. Electrochem. 4 (2017) 190–198.
[13] J. Babauta, R. Renslow, Z. Lewandowski, H. Beyenal, Electrochemically active biofilms: facts and fiction. A review, Biofouling 28 (2012) 789–812.
[14] D. Sun, J. Chen, H. Huang, W. Liu, Y. Ye, S. Cheng, The effect of biofilm thickness on electrochemical activity of Geobacter sulfurreducens, Int. J. Hydrogen Energy 41 (2016) 16523–16528.
[15] N.S. Malvankar, V.M. Rotello, M.T. Tuominen, D.R. Lovley, Reply to 'measuring conductivity of living Geobacter sulfurreducens biofilms', Nat. Nanotechnol. 11 (2016) 913–914.
[16] M.D. Yates, S.M. Strycharz-Glaven, J.P. Golden, J. Roy, S. Tsoi, J.S. Erickson, M.Y. El-Naggar, S.C. Barton, L.M. Tender, Measuring conductivity of living Geobacter sulfurreducens biofilms, Nat. Nanotechnol. 11 (2016) 910–913.
[17] C. Li, K.L. Lesnik, Y. Fan, H. Liu, Millimeter scale electron conduction through exoelectrogenic mixed species biofilms, FEMS Microbiol. Lett. 363 (2016).
[18] N.S. Malvankar, M. Vargas, K.P. Nevin, A.E. Franks, C. Leang, B.C. Kim, K. Inoue, T. Mester, S.F. Covalla, J.P. Johnson, V.M. Rotello, M.T. Tuominen, D.R. Lovley, Tunable metallic-like conductivity in microbial nanowire networks, Nat. Nanotechnol. 6 (2011) 573–579.
[19] H.S. Lee, B.R. Dhar, J. An, B.E. Rittmann, H. Ryu, J.W. Santo Domingo, H. Ren, J. Chae, The roles of biofilm conductivity and donor substrate kinetics in a mixed-culture biofilm anode, Environ. Sci. Technol. 50 (2016) 12799–12807.
[20] C. Li, K.L. Lesnik, Y. Fan, H. Liu, Redox conductivity of current-producing mixed species biofilms, PLoS ONE 11 (2016)e0155247.
[21] M.D. Yates, B.J. Eddie, N. Lebedev, N.J. Kotloski, S.M. Strycharz-Glaven, L.M. Tender, On the relationship between long-distance and heterogeneous electron transfer in electrode-grown Geobacter sulfurreducens biofilms, Bioelectrochemistry 119 (2018) 111–118.
[22] J.T. Babauta, H.D. Nguyen, T.D. Harrington, R. Renslow, H. Beyenal, pH, redox potential and local biofilm potential microenvironments within Geobacter sulfurreducens biofilms and their roles in electron transfer, Biotechnol. Bioeng. 109 (2012) 2651–2662.
[23] A. Mohamed, P.T. Ha, B.M. Peyton, R. Mueller, M. Meagher, H. Beyenal, In situ enrichment of microbial communities on polarized electrodes deployed in alkaline hot springs, J. Power Sources 414 (2019) 547–556.
[24] E. Marsili, J.B. Rollefson, D.B. Baron, R.M. Hozalski, D.R. Bond, Microbial biofilm voltammetry: direct electrochemical characterization of catalytic electrode-attached biofilms, Appl. Environ. Microbiol. 74 (2008) 7329–7337.
[25] J.R. Lloyd, C. Leang, A.L. Hodges Myerson, M.V. Coppi, S. Cuifo, B. Methe, S.J. Sandler, D.R. Lovley, Biochemical and genetic characterization of PpcA, a periplasmic c-type cytochrome in Geobacter sulfurreducens, Biochem. J. 369 (2003) 153–161.
[26] M.D. Yates, J.P. Golden, J. Roy, S.M. Strycharz-Glaven, S. Tsoi, J.S. Erickson, M.Y. El-Naggar, S. Calabrese Barton, L.M. Tender, Thermally activated long range electron transport in living biofilms, Phys. Chem. Chem. Phys. 17 (2015) 32564–32570.
[27] R.M. Snider, S.M. Strycharz-Glaven, S.D. Tsoi, J.S. Erickson, L.M. Tender, Long-range electron transport in Geobacter sulfurreducens biofilms is redox gradient-driven, Proc. Natl. Acad. Sci. U. S. A. 109 (2012) 15467–15472.
[28] N.S. Malvankar, M.T. Tuominen, D.R. Lovley, Lack of cytochrome involvement in long-range electron transport through conductive biofilms and nanowires of Geobacter sulfurreducens, Energy Environ. Sci. 5 (2012).
[29] S.M. Strycharz-Glaven, L.M. Tender, Reply to the 'Comment on "On electrical conductivity of microbial nanowires and biofilms"' by N. S. Malvankar, M. T. Tuominen and D. R. Lovley, Energy Environ. Sci., 2012, 5, DOI: 10.1039/c2ee02613a, Energy Environ. Sci. 5 (2012).
[30] R.J. Steidl, S. Lampa-Pastirk, G. Reguera, Mechanistic stratification in electroactive biofilms of Geobacter sulfurreducens mediated by pilus nanowires, Nat. Commun. 7 (2016) 12217.
[31] K. Inoue, C. Leang, A.E. Franks, T.L. Woodard, K.P. Nevin, D.R. Lovley, Specific localization of the c-type cytochrome OmcZ at the anode surface in current-producing biofilms of Geobacter sulfurreducens, Environ. Microbiol. Rep. 3 (2011) 211–217.
[32] D.J. Filman, S.F. Marino, J.E. Ward, L. Yang, Z. Mester, E. Bullitt, D.R. Lovley, M. Strauss, Structure of a cytochrome-based bacterial nanowire, bioRxiv, 2018, 492645.
[33] Cell 177 (2) (2019) 361–369.e10, https://doi.org/10.1016/j.cell.2019.03.029.
[34] B. Virdis, F. Harnisch, D.J. Batstone, K. Rabaey, B.C. Donose, Non-invasive characterization of electrochemically active microbial biofilms using confocal Raman microscopy, Energy Environ. Sci. 5 (2012) 7017.
[35] B.R. Dhar, J. Sim, H. Ryu, H. Ren, J.W. Santo Domingo, J. Chae, H.S. Lee, Microbial activity influences electrical conductivity of biofilm anode, Water Res. 127 (2017) 230–238.